

NUMERICAL INVESTIGATION OF WALL HEAT TRANSFER IN TURBULENT REACTING WALL-JETS

Zeinab Pouransari and Arne V. Johansson
Linné FLOW Centre, Dept. of Mechanics,
Royal Institute of Technology
SE-100 44 Stockholm, Sweden
zeinab@mech.kth.se

ABSTRACT

In the present investigation, three-dimensional direct numerical simulation is used to study a binary irreversible exothermic global reaction in a plane turbulent wall-jet. The flow is compressible and the chemical reaction is modeled by a single-step reaction with Arrhenius-type reaction rate. A constant coflow velocity is applied above the jet, with a temperature equal to that of the wall and a temperature dependent viscosity according to Sutherland's law is used. At the inlet, fuel and oxidizer enter the domain separately in a non-premixed manner. The inlet Reynolds and Mach numbers are the same in all simulation cases. Primarily, it is observed that heat release effects delay the transition and the growth rate of the turbulent wall-jet is influenced by the reaction through temperature-induced changes and density variations. The wall heat flux is increased, however the corresponding Nusselt numbers decrease with increase of heat release.

INTRODUCTION

Combustion systems in confined domains in addition to the strong multi-scale and non-linear dynamics involved, contain regions with flame-wall and turbulent-wall interactions. Thus better understanding of the wall effects plays an essential role in gaining insight into the full problem. The turbulent wall-jet configuration is a unique case which includes turbulence-wall interaction and also has a close resemblance to practical applications. Small scales of turbulence are present close to the wall whereas larger scales exist in the outer shear region. This makes the turbulent wall-jet a valuable test case for reaction and mixing applications. In the past three decades, direct numerical simulation (DNS) has become an essential tool for understanding of turbulent combustion. Since, all the chemical and flow scales are resolved in DNS, the resulting data provide unique information for building better turbulent combustion models. Moreover, gaining data in the near-wall region, difficult in experimental measurements, is feasible in DNS studies, see Vervisch & Poinso (1998), Peters (2000) and Pitsch (2006). A single-step global reaction is an estimation for the full chemistry which takes place in real combustion systems, that enables us to gain insight into the fundamental interactions between heat-release and turbulence in a three-dimensional flow field without detailed concerns

about the chemistry. Apart from turbulence-chemistry interaction, flame and wall have strong interaction in the vicinity of walls, where there will be restriction for flame wrinkling due to the geometrical constraints and the flow field will be modified due to enormous changes in viscosity caused by heat-release. The heat release effects have been the subject of many studies, McMurtry *et al.* (1989), Ruetsch *et al.* (1995), Livescu *et al.* (2002) and Knaus & Pantano (2009). However, most of these studies have excluded the wall effects. In cases with the wall interactions a closer look at the fundamental statistics for combustion modeling is necessary. Numerical investigations of wall-bounded reacting flows have been restricted to the case of turbulent boundary layers and turbulent channel flows, see Martin & Candler (2001) and Gruber *et al.* (2010). Reports on simulations of the wall-jet flow, even on non-reacting cases, are still scarce. See Ahlman *et al.* (2007) and Ahlman *et al.* (2009) for DNS of isothermal and non-isothermal wall-jets. In the present study we concentrate on heat-release effects and turbulent-chemistry interactions present in the turbulent wall-jet configuration. In our previous study of the isothermal reacting turbulent wall-jet, Pouransari *et al.* (2011), the influence of turbulent mixing on the reactions was studied in the absence of temperature effects. Here, DNS of turbulent reacting wall-jets including heat release is performed, where a global exothermic reaction is considered. The main objective of this study is to investigate the role of heat release in the chemically reacting turbulent wall-jet flows and its influences on turbulence and reactants statistics. Discussions about the wall heat transfer and the heat release rates in different reacting wall-jet flows are included.

GOVERNING EQUATIONS

The conservation equations of total mass, momentum and energy read

$$\frac{\partial \rho}{\partial t} + \frac{\partial \rho u_j}{\partial x_j} = 0 \quad (1)$$

$$\frac{\partial \rho u_i}{\partial t} + \frac{\partial \rho u_i u_j}{\partial x_j} = -\frac{\partial p}{\partial x_i} + \frac{\partial \tau_{ij}}{\partial x_j} \quad (2)$$

$$\frac{\partial \rho E}{\partial t} + \frac{\partial \rho E u_j}{\partial x_j} = \dot{\omega}_T + \frac{\partial q_i}{\partial x_i} + \frac{\partial (u_i (\tau_{ij} - p \delta_{ij}))}{\partial x_j}. \quad (3)$$

Here ρ is the total mass density, u_i are the velocity components, p is the pressure, $E = e + \frac{1}{2}u_i u_i$ is the total energy and $\dot{\omega}_T$ is the heat release term due to combustion. The summation convention over repeated indices is used. The heat fluxes q_i are approximated by Fourier's law $q_i = -\lambda \frac{\partial T}{\partial x_i}$, where λ is the coefficient of thermal conductivity and T is the temperature. The viscous stress tensor is defined as $\tau_{ij} = \mu \left(\frac{\partial u_i}{\partial x_j} + \frac{\partial u_j}{\partial x_i} \right) - \mu \frac{2}{3} \frac{\partial u_k}{\partial x_k} \delta_{ij}$, where μ is the dynamic viscosity. The fluid is assumed to be calorically perfect and to obey the ideal gas law according to $e = c_v T$, $p = \rho R T$, and a specific heat ratio of $\gamma = c_p/c_v = 1.4$ is used. The viscosity is determined through the Sutherland's law

$$\frac{\mu}{\mu_j} = \left(\frac{T}{T_j} \right)^{3/2} \frac{T_j + S_0}{T + S_0}, \quad (4)$$

where T is the local temperature, T_j is the jet center temperature at the inlet and $S_0 = 110.4K$ is a reference value. Conservation of the species masses is governed by

$$\frac{\partial \rho \theta_k}{\partial t} + \frac{\partial}{\partial x_j} (\rho \theta_k u_j) = \frac{\partial}{\partial x_j} \left(\rho \mathcal{D} \frac{\partial \theta_k}{\partial x_j} \right) - \dot{\omega}_k \quad (5)$$

where θ_k and $\dot{\omega}_k$ are the mass fractions and the reaction rate of the oxidizer, fuel and passive scalar species. Binary diffusion, with an equal diffusion coefficient \mathcal{D} for all scalars, is used to approximate the diffusive fluxes.

The reaction is modeled as a single-step irreversible reaction between oxidizer species O and fuel species F that react to form a product P and is described as $O + rF \rightarrow (1+r)P$. Stoichiometric coefficients of one are used for all species, i.e. $r = 1$. This implies that the reaction rates for all the reactants are equal. The molecular weights are also assumed to be equal for the reactants and hence the reaction mass rates of the species are formulated as $\dot{\omega}_o = \dot{\omega}_f = \dot{\omega} = -\frac{1}{r+1} \dot{\omega}_p$. An Arrhenius-type reaction rate is assumed. Since $r = 1$, the source term in the product species equation becomes

$$\dot{\omega}_p = -Da \rho^2 \theta_o \theta_f \exp(-Ze/T). \quad (6)$$

The combustion heat release term, $\dot{\omega}_T$, is related to the species reaction rate terms by $\dot{\omega}_T = -\sum_{k=1}^N \Delta h_{f,k}^0 \dot{\omega}_k$ where $\Delta h_{f,k}^0$ is the formation enthalpy of the k^{th} -species. Due to the linear relation between different reaction-rate terms, $\dot{\omega}_T$ is formulated as

$$\dot{\omega}_T = \frac{Ce}{(\gamma-1)M_0^2} \dot{\omega}_p. \quad (7)$$

The chemical reaction is prescribed by a number of non-dimensional numbers, namely the Damköhler number, $Da = \frac{\tau_{conv}}{\tau_{react}} = \frac{h}{U_j} k_r \rho_j$, the Zeldovich number, $Ze = E_a/RT_j$, and the heat release parameter, $Ce = -H^0/c_p T_j$. Here, $-H$ is the heat of reaction, k_r is the reaction-rate constant and E_a is the activation energy of the chemical reaction. In addition, U_j and ρ_j are the centerline velocity and the density of the jet at the inlet. Apart from the oxidizer and fuel, a passive scalar equation is also solved for.

NUMERICAL METHOD AND PARAMETERS

Table 1. Parameters for DNS of reacting turbulent wall-jets; $M_0 = 0.5$, $Pr = 0.7$, $Sc = 0.7$ and $Re = 2000$ in all simulations.

Case	Description	Ce	Da	Ze	Line style
I	Isothermal	0	3	0	—
II	heat-release	10	3	0	...
III	Arrhenius-type	25	1100	8	---
IV	Arrhenius-type	25	1900	8	---

A fully compressible Navier-Stokes solver is employed for the simulations. The code uses a sixth order compact finite difference scheme for spatial discretization and a third order Runge-Kutta method for the temporal integration. The computational domain is a rectangular box, the size of which in terms of inlet jet height h , is $(L_x = 35h) \times (L_y = 17h) \times (L_z = 7.2h)$ where x , y and z denote the streamwise, wall-normal and spanwise directions, respectively. The number of grid points used in the simulation are $(N_x = 320) \times (N_y = 192) \times (N_z = 128)$. Statistics are computed by ensemble averaging over time and the periodic spanwise direction. Reynolds number is defined as $Re = U_j h / \nu_j$, where subscript j denotes properties at the inlet jet center. Mach and Schmidt numbers are defined as $M = U_j / a$ and $Sc = \nu / \mathcal{D}$, respectively, where ν is the kinematic viscosity and a is the speed of sound. The initial temperature of the jet stream, coflow and the wall are equal to $T_j = T_w = 750(K)$. The ambient flow above the jet has a constant coflow velocity of $U_c = 0.10U_j$. For the heat fluxes, a constant Prandtl number $Pr = \mu c_p / \lambda = 0.72$ is used. The Schmidt number of the scalars is also constant and equal to the Prandtl number, i.e. $Sc = \mu / \rho D = 0.72$. At the inlet, fuel and oxidizer enter the domain separately in a non-premixed manner, fuel is injected through the jet, $\theta_{f,j} = 1$, while the oxidizer is injected in the coflow, $\theta_{o,c} = 0.5$. To specify the reaction rates, Damköhler numbers $Da = h k_r \rho_j / U_j$ of different values are used. The Da number defines the ratio of the convection to reaction time scale in terms of inlet properties. To prevent the reflection and generation of waves, sponge zones are implemented at the inlet and outlet boundaries. For many other numerical issues, concerning the high wave number disturbances, accumulation of negative concentrations, the transition to turbulence and details of the boundary conditions, see the work by Ahlman *et al.* (2009) and Pouransari *et al.* (2011).

Two different sets of heat-release simulations are performed. In the first DNS, case II, a simplified reaction term is considered which is a function of density and reactant concentrations and does not depend on temperature, however it appears as a source term in the energy equation. This is similar to the heat release study of McMurtry *et al.* (1989) on shear flows. Despite the simplified formulation of the reaction-rate term in this simulation, many of the significant influences of heat-release on flow dynamics can still be observed. The second set of simulations, cases III and IV, use an Arrhenius-type formulation, as described in eq. (6) for the reaction-rate term. Parameters for DNS of reacting turbulent wall-jets for all simulation cases are presented in Table 1. The parameters

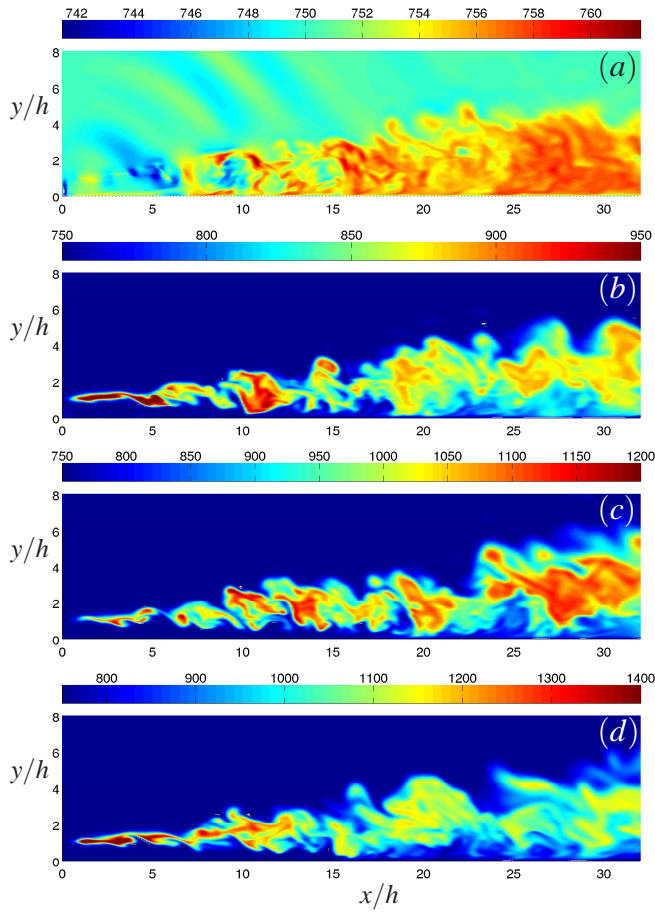


Figure 1. Snapshots of temperature field for (a) case I (b) case II (c) case III (d) case IV.

used in the DNS by Pouransari *et al.* (2011) are also presented there, case I, since we are going to compare turbulence statistics to those from that simulation. Note that the line styles indicated in Table 1 are used throughout the paper unless otherwise stated. Two simulation cases, III and IV possess identical numerical parameters except for the Damköhler number. Thus, its effects on the temperature rise and the influences on the flame structure will be addressed.

JET DEVELOPMENT

The statistics of the turbulent jet development in four cases, I to IV, are presented below. To provide an overview of both the jet structure and heat release influences in the simulations, snapshots of the instantaneous temperature fields are presented in figure 1. The flow structure and the temperature rises and the temperature distributions are distinctly different for the different cases. The flow is from left to right and is evolving in space and the temperatures are given in Kelvin.

The reaction starts immediately after the inlet and continues downstream. A significant amount of heat is released and the flame is formed already at the jet inlet. As observed in figures 1 (b), (c) and (d) large temperature variations occur due to the chemical reaction. Heat-release effects modify the flow field and high temperatures influence the development and dynamics of the wall-jet through density changes which

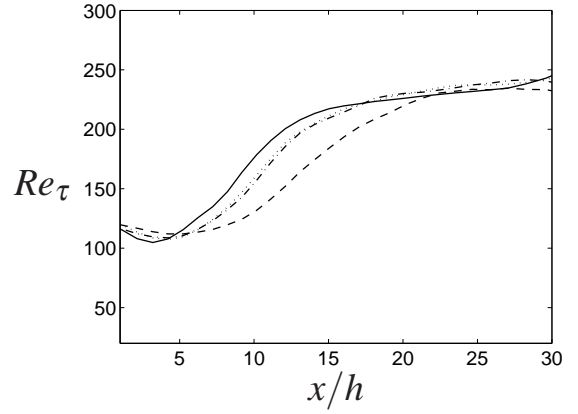


Figure 2. Downstream development of the friction Reynolds number.

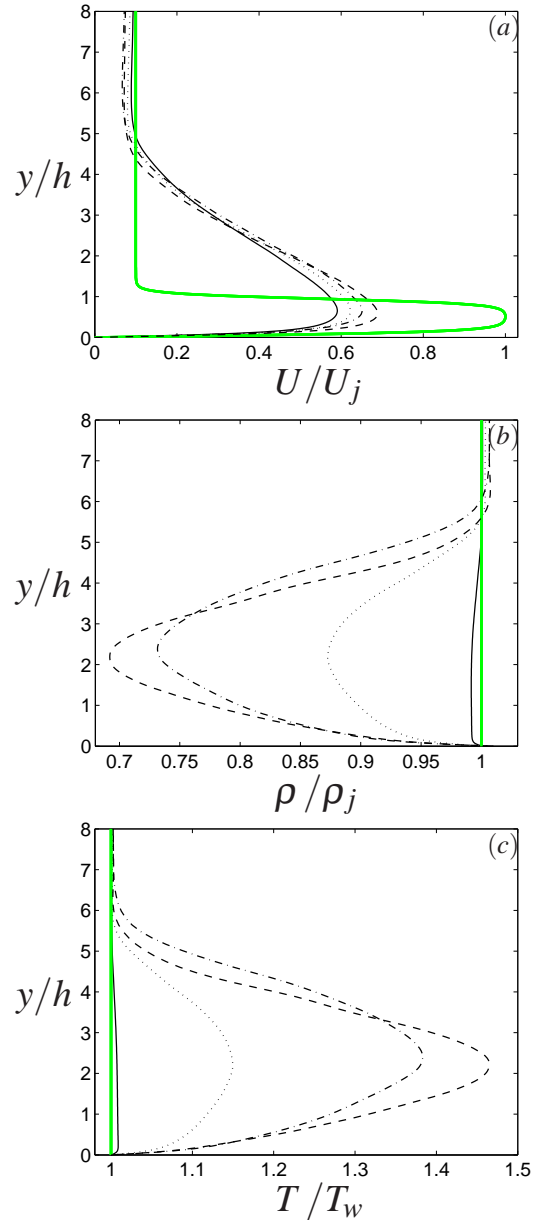


Figure 3. Mean cross-stream profiles of (a) velocity, (b) density and (c) temperature at downstream position $x/h = 25$; The respective profiles at inlet are shown in thick solid green.

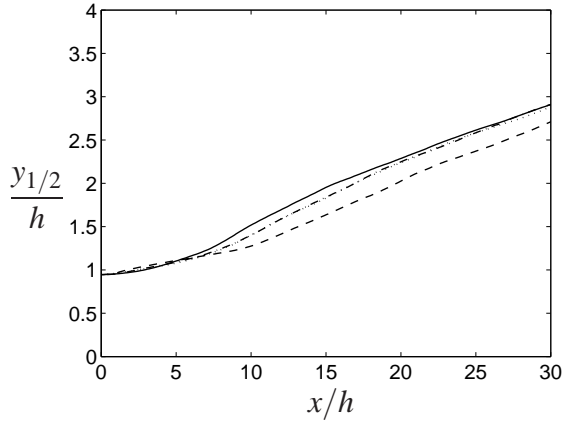


Figure 4. Downstream development of the jet half-height.

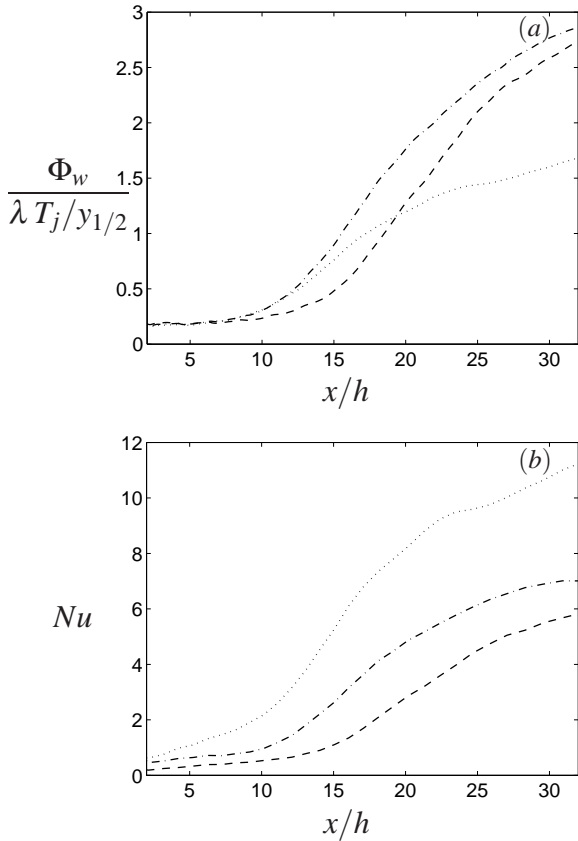


Figure 5. Downstream development of (a) wall heat flux in the absolute scales (b) corresponding Nusselt numbers.

are caused by gas expansion and viscosity changes. These differences in turbulence structures may have a significant influence on for example the heat transfer to the wall in cooling and combustion applications. An understanding of the origins of the differences can be obtained by examining the friction Reynolds number,

$$Re_\tau = \frac{\delta}{l^*} = \frac{u_\tau \delta}{\nu_w} = \frac{\delta}{\nu_w^{1/2}} \sqrt{\left(\frac{dU}{dy}\right)_{y=0}}. \quad (8)$$

When an appropriate outer length-scale δ is used, the friction Reynolds number provides an estimate of the outer-layer to inner-layer length-scale ratio. Figure 2 shows that there are significant differences between exothermic and isothermal reacting wall-jets. Considering downstream position $x/h = 15$, where the isothermal reacting case has approximately reached $Re_\tau = 220$, the chemically reacting cases exhibit much lower values, e.g. $Re_\tau = 170$ for case IV, which reaches $Re_\tau = 220$ only after $x/h = 24$. Thus, figure 2 indicates that transition to turbulence is delayed due to the heat release effects. A higher friction velocity can be caused by an increase in kinematic viscosity or an increase in the velocity gradients at the wall. As we impose an isothermal wall boundary condition, the viscosity is constant for different cases, but $\left(\frac{\partial U}{\partial y}\right)_{wall}$ is increasing with increasing heat release. That is partly due to the increase in average velocity of the jet at downstream positions, see figure 3(a).

Cross-stream profiles of the velocity, temperature and density are shown in figure 3. As is illustrated in figure 3 (b), the density changes in the chemically reacting cases are significant and the average density may reach values as low as almost half of the inlet value. The maximum of the average mean velocity of the wall-jet increases by adding heat-release throughout the region. This is due to thermal expansion caused by the chemical reaction which increases the volume flux and thus the maximum velocity will increase.

The wall-jet growth is depicted in figure 4 in terms of the development of the jet half-height $y_{1/2}$, defined as the position in the outer shear layer where the velocity attains half the maximum excess value, i.e. $U(y_{1/2}) = (U_m - U_c)/2$. Previous studies of incompressible wall-jets and also non-isothermal compressible wall-jets, show a linear half-height growth of the wall-jet, which is about 20 – 30% lower than those of plane jets, (Launder & Rodi 1981; Dejoan & Leschziner 2005; Ahlman *et al.* (2009)). The linear growth is also found to hold for the chemically reacting jets. However, the half-height of the jet decreases with increase in the heat release. For instance, at $x/h = 20$, the half-height of the jet in case IV is about 11% lower than that of the isothermal reacting wall-jet. This can mainly be ascribed to a delayed transition to turbulence.

WALL HEAT TRANSFER

The instantaneous wall heat flux, ϕ_w , is defined as

$$\Phi_w = -\lambda \left(\frac{dT}{dy}\right)_{wall} \quad (9)$$

where y is the wall-normal direction, T is the gas mixture temperature and λ is the thermal conductivity of the gaseous mixture. The mean heat flux into the solid surface is mainly associated to the hot products which formed along the wall downstream of the jet inlet. The cold wall acts as a heat sink and a large amount of the thermal energy released by chemical reaction is transferred into the solid surface. The mean normalized wall heat fluxes, $\Phi_w / (\lambda T_j / y_{1/2})$, for all chemically reacting cases are shown in figure 5(a). The heat transfer to the wall is increasing by increase in the amount of thermal energy release, i.e. with the enlargement of the chemical source

term. Since the half-height of the jets are comparably weakly modified by the heat release effects, thus the behavior is the same, using any other outer length scale. The resulting effective heat transfer to the wall in the chemically reacting jets can be assessed by computing the corresponding Nusselt number,

$$Nu = \frac{\overline{\Phi_w}}{\lambda \Delta T / y_{1/2}}, \quad (10)$$

where $y_{1/2}$ is the corresponding half-height of each jet and ΔT denotes a comparable temperature difference in the average temperature profile of each chemically reacting jet at the particular downstream position. The choice of ΔT makes a meaningful difference in the resulting computed Nusselt numbers for different chemically reacting jets. We have chosen $\Delta T = T_m - T_w$, where T_w is the solid surface temperature, equal in all cases, and T_m is the maximum of the mean temperature profile. It can be seen in figure 5(b) that the corresponding Nusselt number is decreasing with increase in heat release, i.e. $Nu_{II} > Nu_{III} > Nu_{IV}$. And again, the trend is the same using any other outer length scale for computing the Nusselt number. This is due to the fact that even though the absolute value of heat flux is increasing, the maximum temperature in the mean profile is also increasing for cases II to IV, see figure 3(c), which results in decrease of the Nusselt number. In other words, the effective heat transfer to the wall is reduced for cases with higher heat release, due to reduced turbulent mixing. It can be seen in both figures 5(a) and (b), that the wall heat transfer is substantially enhanced at the laminar-to-turbulence transition position, around $x/h = 15$ for all cases. In the isothermal reacting case, an overshoot exist in the transition point, not shown, which is not the case for chemically reacting wall-jets. However, the qualitative behavior of the friction coefficient in chemically reacting cases is similar to that of the isothermal reacting jet, except that the overshoot in the transition point is reduced with increase of heat release.

REACTION RATES

Heat release is generated by the chemical reactions and the reaction depends on mixing and turbulence statistics, e. g. scalar dissipation rates, but it also depends on the prescribed parameters in the global reaction model. The simulation cases with rather similar temperature rise may still have very different flame shapes. The snapshots of the reaction term for cases III and IV, with different Damköhler numbers are presented in figure 6, which shows that the flame gets thinner as the Damköhler number increases. The structure of the flame is affected both in the outer layer, close to the half-height of the jet and in the near-wall region, see figure 6(a) and (b). These plots also show that the reaction mainly occurs in the upper shear layer in thin sheet-like structures; However, reactions also take place near the wall, but to a lesser extent. The absence of a sharp mean gradient implies that the typical streaky pattern near the wall, seen for the velocity, is not formed for the scalars. Instead, turbulent patches of high concentrations of oxidizer are pumped toward the wall, which result in formation of spots of high reaction rates close to the wall. This is demonstrated in figure 6(c) and (d) for the xz -plane at $y^+ = 40$. This is a common behavior in the near-wall region also at lower y^+ -values, but the closer to the wall the fewer

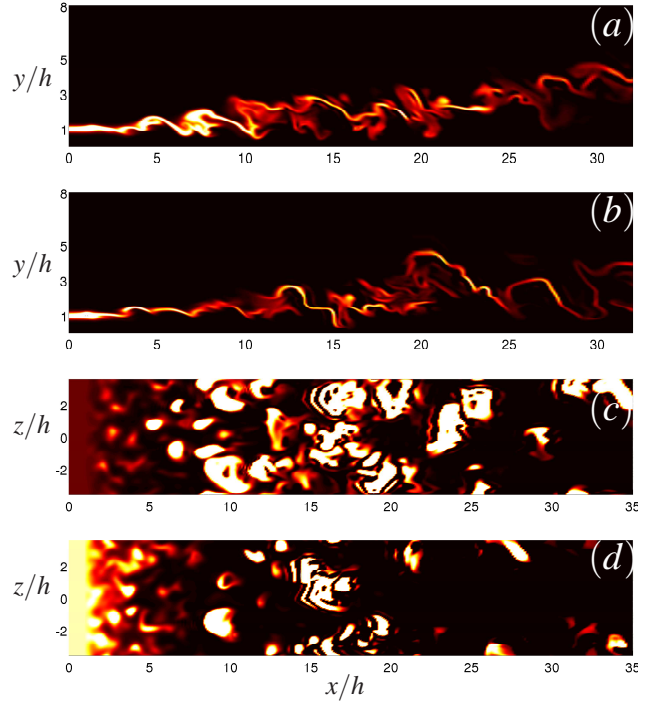


Figure 6. Snapshot of the reaction rate in xy -plane for (a) case III (b) case IV; and xz -plane at constant position from the wall, $y/h = 1/2$, for (c) case III (d) case IV, the two snapshots for each simulation show the same time instant; The lighter color indicates higher reaction rate.

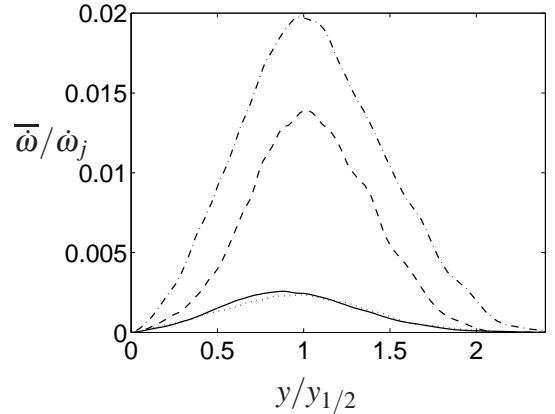


Figure 7. Inlet normalized reaction rate at $x/h = 25$.

spots are observed. The effect of Damköhler number is also seen in these figures, in two plots for case III and IV, it can be seen that the spots of reaction are more spread and distributed for case III, with lower Da number and are somehow more confined and intensified for case IV, with higher Da number.

The inlet normalized mean mass reaction for all reacting cases at downstream position, $x/h = 25$ are shown in figure 7. The reaction rate is normalized by the corresponding inlet value for each simulation case, $\dot{\omega}_j = Da \rho_j^2 \Theta_{o,j} \Theta_{f,j} \exp(-Ze/T_j)$. The reaction mainly takes place around the $y = y_{1/2}$ plane. This is also consistent with the snapshot of the reaction rate which was shown in figure 6. The reaction is thus predominantly found where the reactant

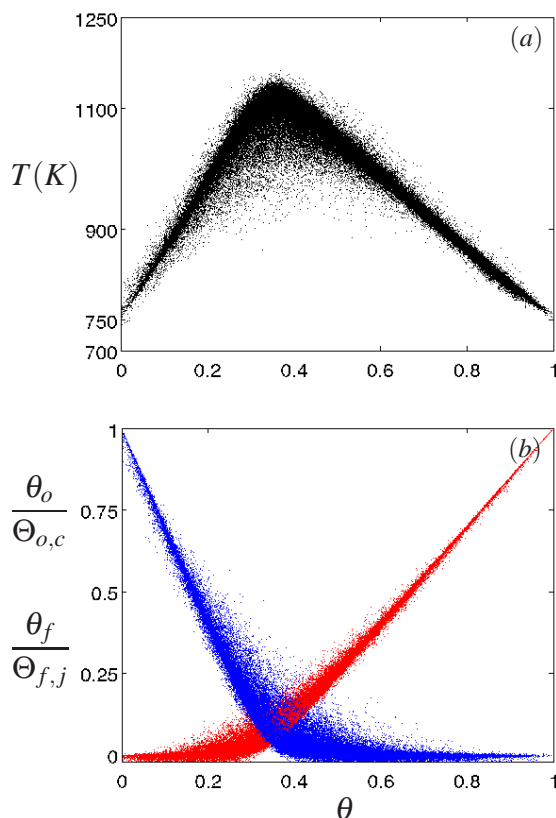


Figure 8. Scatter plots of (a) temperature (b) reacting species, oxidizer (blue) and fuel (red) against mixture fraction at downstream position $x/h = 25$, for case III.

concentrations are high rather than at the position of maximum mixing. The normalized reaction rates collapse for cases I and II, which shows that although the temperature independent source term in the energy equation for case II, can change the temperature field but it cannot significantly influence the overall rate of the reaction. Introducing temperature dependent reactions rates through Arrhenius-type formulation for cases III and IV, increases the reaction rate dramatically. Despite having higher Damköhler number, case IV seems to have lower reaction rate. This is consistent with what is observed for the shape of the flames in figure 6.

The computed scatter plots of the local temperature and the reacting species concentrations against mixture fraction at downstream position $x/h = 25$ are displayed in figure 8. A scatter plot can suggest various kinds of correlations between variables. One of the most powerful aspects of a scatter plot, however, is its ability to show nonlinear relationships between variables. Significant dispersions are observed at all positions. Although the width of the scatter band becomes narrower by moving toward downstream positions but still a substantial scatter is observed at this location. A similar behavior has previously been reported in jet flames, Cao *et al.* (2005), and is attributed to the effect of local strain.

CONCLUSIONS

The present study concerns the role of heat release in the chemically reacting turbulent wall-jet flows. Heat release ef-

fects are studied in several chemically reacting wall-jets using a global reaction model together with three-dimensional direct numerical simulation. Significant variations in the density and temperature fields are observed. The influence of heat release on turbulence and reactants statistics is addressed. The results were compared to the isothermal reacting wall-jet flow at the same inlet Reynolds and Mach numbers, defined at the jet center. Primarily, it is observed that heat release effects delay the transition to turbulence and the growth rate of the turbulent wall-jet is influenced by the reaction through temperature-induced changes and density variations. The wall heat flux is increased due to the substantial temperature rise in the flow field, however, the effective heat transfer to the solid surface, i.e. the corresponding Nusselt number is decreasing with increase of heat release. The snapshots of the reaction term for cases with different Damköhler number show the expected behavior with a thinner flame with increasing Damköhler number. The plots also show that the reaction mainly occurs in the upper shear layer but also take place near the wall. The frequency of the reaction spots in the near-wall region is observed to be directly related to the global Damköhler number.

ACKNOWLEDGEMENTS

The financial support from the Swedish Centre for Combustion Science and Technology (CECOST) and the computer time provided by Swedish National Infrastructure for Computing (SNIC) are gratefully acknowledged. Prof. Bendiks Jan Boersma is thanked for providing the original version of the DNS code.

REFERENCES

- Peters, N. (2000) Turbulent combustion, *Cambridge University Press*.
- Vervisch, L. & Poinso, T. (1998) Direct numerical simulation of non-premixed turbulent flames, *Ann. Rev. Fluid Mech.* **30**, (655–691).
- Pitsch, H. (2006) Large-eddy simulation of turbulent combustion. *Ann. Rev. Fluid Mech.* **38**, pp. 453482.
- McMurtry, P. A., Riley, J. J. & Metcalfe, R. W. (1989) Effects of heat release on the large-scale structure in turbulent mixing layers. *J. Fluid Mech.* **199**, 297332.
- Ruetsch, G. R., Vervisch, L. & Linan, A. (1995) Effects of heat release on triple flames, *Phys. Fluids* **7**, (1447–1454).
- Livescu, D., Jaber, F. A. & Madnia, C. K. (2002) The effects of heat release on energy exchange in reacting turbulent shear flow, *J. Fluid Mech.* **450**, (35–66).
- Knaus, R. & Pantano, C. (2009) On the effect of heat release in turbulence spectra of non-premixed reacting shear layers, *J. Fluid Mech.* **626**, (67–109).
- Martin, M. P. & Candler, G. V. (2001) Temperature-fluctuation scaling in reacting boundary layers, *Center for Turbulence Research, Annual Research Briefs*, (151–162).
- Gruber, A., Sankaran, R., Hawkes, E. R. & Chen, J. H. (2010) Turbulent flame-wall interaction: a direct numerical simulation study, *J. Fluid Mech.* **658**, (5–32).
- Ahlman, D., Brethouwer, G. & Johansson, A. V. (2007) Direct numerical simulation of a plane turbulent wall-jet including scalar mixing. *Phys. Fluids*, **19**, 065102.
- Ahlman, D., Velter, G., Brethouwer, G., & Johansson, A. V. (2009) Direct numerical simulation of non-isothermal turbulent wall-jets. *Phys. Fluids*, **21**, 035101.
- Pouransari, Z., Brethouwer, G. & Johansson, A. V. (2011) Direct numerical simulation of a reacting turbulent wall-jet. Submitted.
- Dejoan, A. & Leschziner, M. A. 2005 Large eddy simulation of a plane turbulent wall jet. *Phys. Fluids* **17**, 025102.
- Launder, B. E. & Rodi, W. 1981 The turbulent wall jet. *Prog. Aerospace. Sci* **19**, 81128.
- Cao, R. R., Pope, S. B. & Masri, A. R. (2005) Turbulent lifted flames in a vitiated coflow investigated using joint pdf calculations. *Combust. Flame* **142**, 438453.
- Boersma, B. J. (1999) Direct numerical simulation of a turbulent reacting jet. *Center for Turbulence Research, Annual Research Briefs*, 59-72.